Macromolecules

pubs.acs.org/Macromolecules Article

Covalent Adaptable Networks with Rapid UV Response Based on Reversible Thiol−Ene Reactions in Silicone Elastomers

Miao Huo, Jerry G. Hu, and David R. Clarke*

Cite This: https://doi.org/10.1021/acs.macromol.3c01841 Read Online

ACCESS | Metrics & More | Article Recommendations | Supporting Information

ABSTRACT: PhotoCAN silicone elastomers, based on the thiol−ene reaction, exhibit rapid and reversible changes in dynamic modulus at room temperature when illuminated by UV. By combining results from magic angle spinning solid-state NMR as well as EPR and rheometry measurements, both under UV, it is concluded that the mechanical response can be attributed to a combination of dissociative, associative, and oxidation reactions. The cleavage of the C−S bonds under UV in the presence of an excess of thiyl radicals is identified as the reversible dissociative reaction responsible for abrupt drops in the storage modulus. A slower but concurrent reaction is a termination process involving thiyl radicals to form disulfide bonds. A kinetic model is developed that successfully relates the rates of the underlying reaction mechanisms to changes in the storage modulus. The results provide a basis for designing new, ambient temperature photoresponsive covalently adaptive network materials.

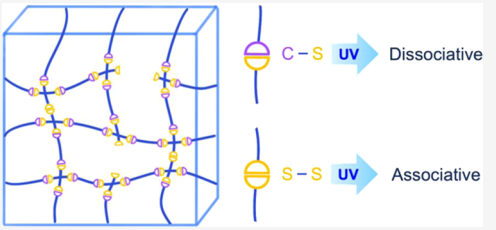

1. INTRODUCTION

Covalent adaptive network (CAN) polymers have the ability to adapt their structure and properties in response to changes in their environment, typically temperature changes, enabling them to function as smart materials.[1−4] They can be synthesized by using a variety of different approaches, giving researchers a high degree of control over their properties and behavior. Recently, there has been growing interest in the use of sulfur as a core element in CAN polymers.[3] Sulfur-containing polymers offer several advantages, including enhanced thermal stability and greater resistance to oxidation, usually without the need for catalysts.[5,6] Researchers have also found that sulfur-containing polymers can be synthesized using a range of different methods, including thiol−ene chemistry, which offers a high degree of control over the polymerization process.[3,7]

The convenience of thiol−ene reactions allows for the facile design of elastomer structures. While the thiol−ene reaction is widely recognized as a "click reaction", its reverse reaction has only been discussed in recent years. For instance, Konkolewicz et al. discussed the reverse reaction of thiol−ene under heat and basic conditions[8] and Kalow et al. reported the reversibility of thiolacetal on heating.[9] Meanwhile, Winne et al. described the reversible reaction of thiol−yne cross-linker under heating and base conditions.[3] These studies on reversible thiol−ene and its related reactions provide more options for the use of dynamic construction of novel CANs. However, most of the contributions have considered the reverse reactions of thiol−ene under heating and cooling conditions. The mechanical properties of CANs prepared through thiol−ene reactions have been reported to respond to UV illumination.[10] Yet, the underlying mechanism of the response to UV and possible relationships to thiol−ene reactions have not been thoroughly investigated.

In recent work,[10] we described a series of elastomers, termed photoCANs, prepared using the thiol−ene reaction, which exhibit rapid and reversible modulus changes in response to UV illumination at ambient conditions and with no heating. However, the underlying mechanisms were not elucidated. To design superior elastomers, a deeper understanding of the relationship between the physical properties of photoCAN and the chemical reactions occurring is necessary.

This contribution focuses on understanding how photoCAN elastomers containing both C−S and S−S bonds can be synthesized and how they react under UV. By gaining a better understanding of the fundamental properties and behavior of these materials, we hope to unlock new possibilities for their design and use in a range of different applications.

2. EXPERIMENT

2.1. Materials. Three thiol-PDMS polymers and one vinyl-PDMS polymer were used in this work. The chemical structure of their oligomers is shown in Figure S1. One of the thiol-PDMS was a PDMS with both ends terminated with a thiol group, designated SM21, and had a molecular weight of 10 000 g/mol. The other two thiol-PDMS were mercaptopropyl

Received: September 11, 2023
Revised: October 23, 2023
Accepted: November 1, 2023

https://doi.org/10.1021/acs.macromol.3c01841
Macromolecules XXXX, XXX, XXX−XXX

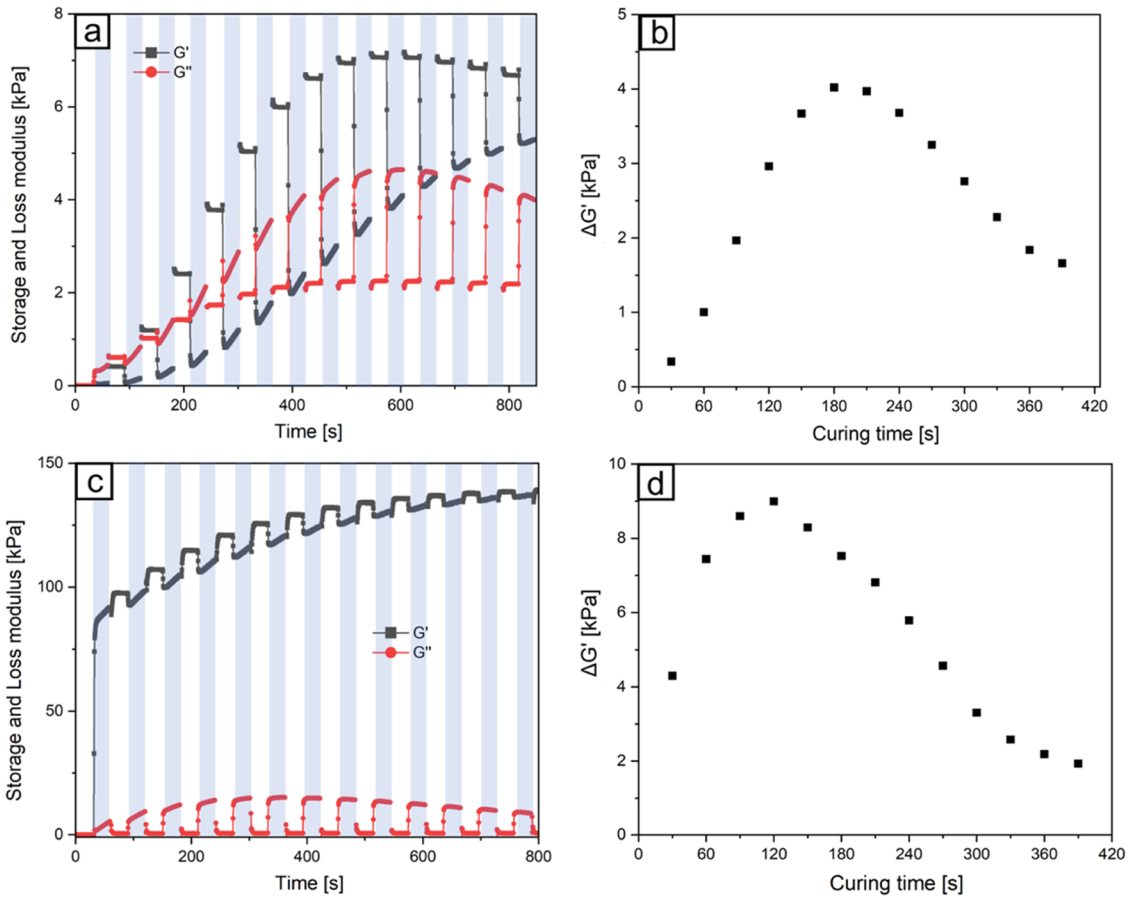

Figure 1. (a) Storage and loss moduli of the S-PDMS elastomer as a function of time. Superimposed, and indicated by the shading are the times during which the material was illuminated by UV. The UV illumination consisted of alternating 30 s on/off cycles at a fluence of 45 mW/cm^2. (b) $\Delta G'$ of S-PDMS as a function of curing time. (c) Variation in storage and loss moduli of H-PDMS over time with periodic UV illumination, shown by the shaded bars. (d) $\Delta G'$ of H-PDMS as a function of curing time.

methylsiloxane-β-dimethylsiloxane copolymers with molecular weights of 6000−8000 g/mol, designated SMS42 and SMS22, respectively. The mole ratio of mercaptopropyl in SMS42 and SMS22 is 4−6 and 2−3%, respectively. The vinyl-PDMS was PDMS with both ends terminated by vinyl. It had a molecular weight of 9400 g/mol and is designated V22. All functional PDMS materials were purchased from Gelest, Inc. The photoinitiator, Irgacure 1173 (2-hydroxy-2-methyl propiophenone), was purchased from Sigma-Aldrich. All of the materials purchased were used without modification.

2.2. Sample Preparation. Two elastomer compositions were prepared, one referred to as S-PDMS and the other as H-PDMS. They were both prepared by mixing the thiol-PDMS and vinyl-PDMS liquids with the photoinitiator at 2000 rpm for 5 min using a Thinky Mixer. The S-PDMS consisted of a mixture of 2.05 g of SMS22, 1.07 g of SM21, 1.34 g of V22, and 1 wt % photoinitiator. After mixing, the resulting liquid was sealed in a vial and covered with aluminum foil to avoid stray light activation by the photoinitiator. The H-PDMS consisted of a mixture of 1.27 g of SMS42, 1.34 g of V22, and 1 wt % photoinitiator. Both stoichiometric ratios of vinyl to thiol for S-PDMS and H-PDMS are 1:3. For the NMR and EPR measurements, samples of the H-PDMS were cured under UV light with an intensity of 3.5 mW/cm^2 for 120, 480, 960, and 2000 s.

2.3. Characterization. For the NMR measurements, samples of H-PDMS were first cured under a protective gas of nitrogen for different times and then measured since the NMR instrument did not have in situ UV illumination capability. The samples were cut into small pieces of the elastomer for solid-state NMR measurements under magic angle spinning (MAS) conditions. The ^{1}H and ^{13}C solid-state MAS NMR measurements were performed on a Bruker DMX 500 MHz (11.7 T) spectrometer, operating at 500.24 and 125.79 MHz for ^{1}H and ^{13}C, respectively, with a 4 mm zirconia rotor system at a spinning frequency of 6 kHz.

The ^{1}H MAS experiments were performed using a 30° excitation pulse of 1.8 μs, a 5 s relaxation delay, an acquisition time of 0.33 ms, and an accumulation of about 200 scans. The ^{13}C MAS experiments were performed using a 30° ^{13}C excitation pulse of 1.02 μs, a 6 s relaxation delay, an acquisition time of 10.24 ms, and an accumulation of over 20,000 scans. A 60 kHz proton decoupling was applied during the 13C data acquisition. The ^{1}H and ^{13}C chemical shifts were both referenced to the TMS standard.

EPR tests were performed on a Bruker EMX X-band EPR instrument. The field was swept from 3240 to 3440 G with a sweep time of about 31 s. The elastomer was contained in standard 4 mm OD and 3 mm ID EPR quartz tube. The sample height was about 2 inches. No additional chemicals were added to the sample for the EPR measurements. The UV illumination (365 nm) at ~95 mW/cm^2 was applied from one side of the tube through a mesh window on the EPR cavity. About 50% of the sample was exposed to UV light.

https://doi.org/10.1021/acs.macromol.3c01841
Macromolecules XXXX, XXX, XXX−XXX

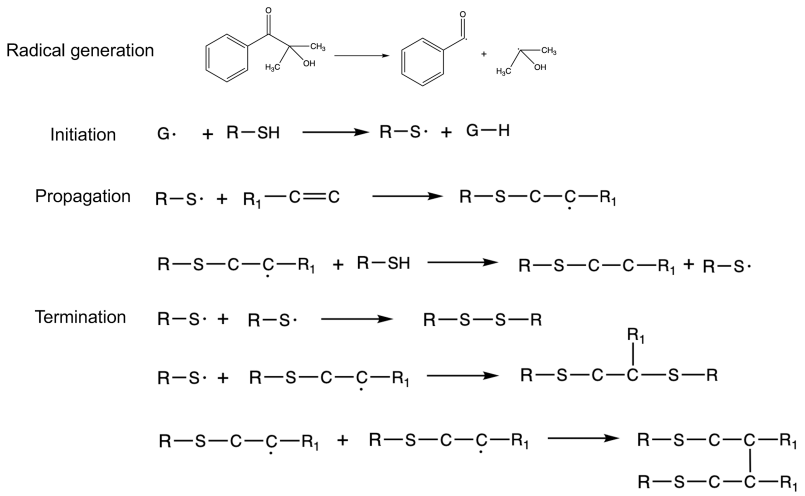

Figure 2. Summary of proposed thiol−ene reactions in CAN polymers reported in the literature.[14] G · is the initial free radical generated by photoinitiator.

Rheology tests were conducted in parallel-plate geometry using a TA HR 20 discovery hybrid rheometer and UV illumination provided by an Omnicure S2000 spot UV curing system. The plate diameter was 20 mm. About 11 drops of uncured samples were dropped onto the lower plate, and a gap of 600 um was set. The UV illumination was set at 320−500 nm for a fluence of 45 mW/cm^2, with the UV light turned on every 60 s for a duration of 30 s. The frequency for the time sweep was 1 Hz, and the maximum shear strain was set to 1%.

3. EXPERIMENTAL RESULTS

3.1. Rheological Results. The unusual UV switching characteristics of the PhotoCAN elastomers are illustrated by the rheological data in Figure 1(a,b) for the S-PDMS elastomer. The data show the evolution of both the storage (G') and loss (G'') moduli with curing time at room temperature. The most striking behavior is the abrupt drop in G' when illuminated by UV and the subsequent switching back to a slightly higher modulus when the UV illumination is turned off. There is a corresponding increase in the G'' when illuminated and a return to the lower, pre-illumination value when the illumination is turned off. As shown in the figure, the magnitude of the UV-induced switching of both the G' and G'' continues to change while the elastomer cures from the initial liquid state to a stiffer material. This is quantified by the data in Figure 1(b) showing the magnitude $\Delta G'$ and the decrement in G' for each exposure to UV, as a function of curing time obtained from Figure 1(a). Initially, the value of $\Delta G'$ is small and then increases, reaching a maximum value followed by a steady decrease with continuing curing until reaching a fully cured state, after which G' no longer responds to UV. There are two other notable features of the G' during the overall curing process. The first is that while illuminated, G' increases almost linearly with time but with a slope that changes with curing time. The second is that in the absence of UV, there is no change in either G' or G''. This is more clearly shown in Figure 1(b). Also, not shown explicitly in the figure, but apparent in the rate of switching, is the time constant associated with these switching changes, typically in seconds, as shown previously.[10]

The observed changes in mechanical properties under UV illumination can be qualitatively understood in terms of polymer network theory such as the affine and phantom models.[11−13] In these models, G' is directly proportional to the effective strand density, ν_{eff}, since not all network strands participate in the deformation process. Strands attached only at one end to the network, termed dangled chains, and loops formed by molecular chains do not resist elastic deformation and are consequently elastically inactive. By contrast, chains fully integrated into the network participate in any deformation. Consequently, the observed changes in G' are a direct measure of changes in the polymer network structure, and the abrupt drop under UV indicates a decrease of the effective strand density.

In the absence of UV light, the polymer system has a high effective strand density and, therefore, a high G'. Furthermore, stiffer surroundings restrict the motion of the polymer chains, resulting in a low G''. In the presence of UV, some of the covalent bonds associated with cross-linking are broken and the intact strands can move more freely because of the lower constraint from the fewer cross-linking points. In turn, this also results in faster relaxation.

The rapid UV-induced switching observed precluded the possibility of examining the structure of the UV-illuminated S-PDMS with post facto NMR measurements since it was not possible to freeze in the illuminated state. In addition, because of the chemical complexity of the S-PDMS structure and the tendency of different atomic nuclei to interact and cause spectral broadening, we chose to use MAS solid-state NMR and obtain ^{13}C and ^{1}H spectra to characterize the molecular structure. Furthermore, to simplify the interpretation of the spectra and reduce unnecessary interferences, we investigated a structurally simpler composition, H-PDMS, which contains only one type of thiol-PDMS (SMS42). Samples were cured for 120, 480, 960, and 2000 s, as well as overcured samples, under a UV intensity of 3.5 mW/cm^2. By observing the changes in various chemical bonds in the system at different curing times, the reaction mechanism is inferred. (The lower UV intensity available for the NMR experiments meant that the curing times are longer than when using the higher UV intensity used in the rheometer).

The rheological data of the simpler H-PDMS polymeric structure are shown in Figure 1(c,d). As shown in Figure 1(c), it exhibits a significantly larger G' than S-PDMS. This is attributed to the absence of thiol-terminated PDMS in H-PDMS and the higher concentration of thiol on SMS42, significantly increasing the density of effective network strands, resulting in a substantial increase in G'. Because of the higher strand density, the material remains highly networked throughout the entire curing reaction. Nevertheless, G' and G'' still change significantly under UV and with magnitudes larger than those for the S-PDMS. Notably, the characteristic features of the UV-induced switching behavior are like those exhibited by the S-PDMS described earlier. $\Delta G'$ as a function of curing time, obtained from Figure 1(c), is shown in Figure 1(d). As with the S-PDMS, the variation increases with curing time in the early stages of the reaction, reaches a maximum, and then decreases with further curing time.

3.2. NMR Measurements. In interpreting our observations, we considered previously proposed reaction mechanisms and products of the thiol−ene reaction. These are shown in Figure 2.[14] Each mechanism leads to the formation of both C−S and disulfide S−S bonds. Disulfide bonds have been previously proposed as being responsible for the thermal and optical response of several CAN-

https://doi.org/10.1021/acs.macromol.3c01841
Macromolecules XXXX, XXX, XXX−XXX

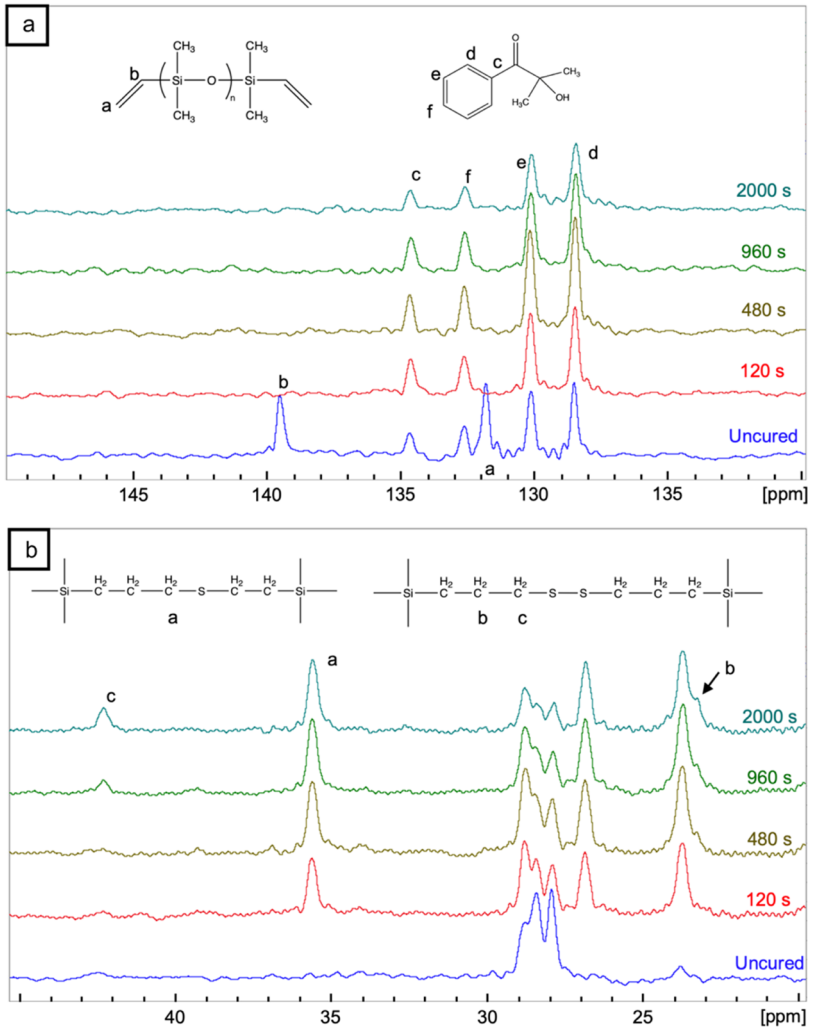

Figure 3. Selected region of the ^{13}C MAS NMR spectra for H-PDMS at the indicated curing times under a UV flux of 3.5 mW/cm^2.

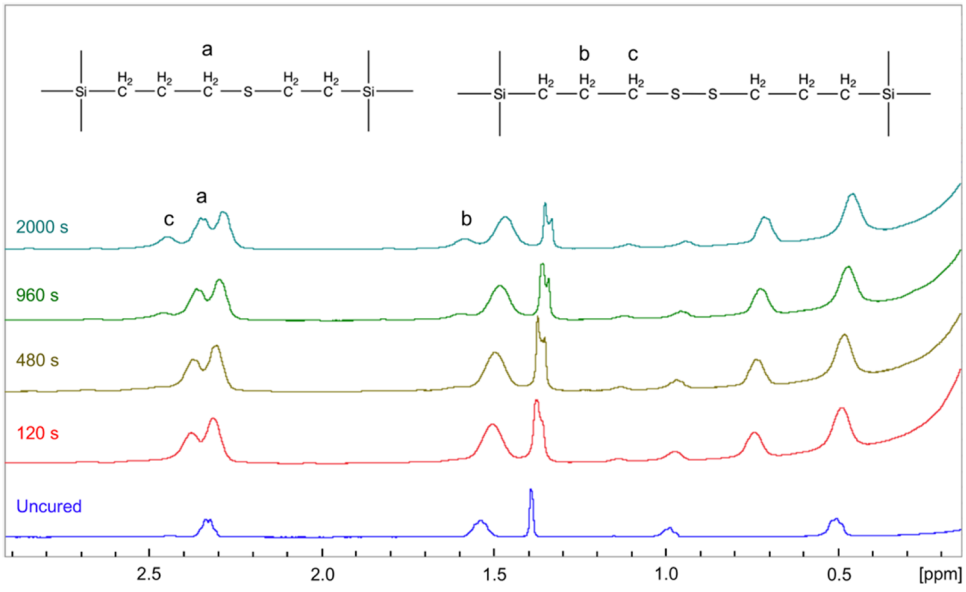

Figure 4. ^1H spectrum of H-PDMS obtained by MAS NMR with increasing curing time.

related polymers[15,16] and C−S bonds have also been reported to be responsible for the CAN response.[17] However, as both of these chemical bonds often occur together in covalently adaptable networks, previous studies have not been able to convincingly

https://doi.org/10.1021/acs.macromol.3c01841
Macromolecules XXXX, XXX, XXX−XXX

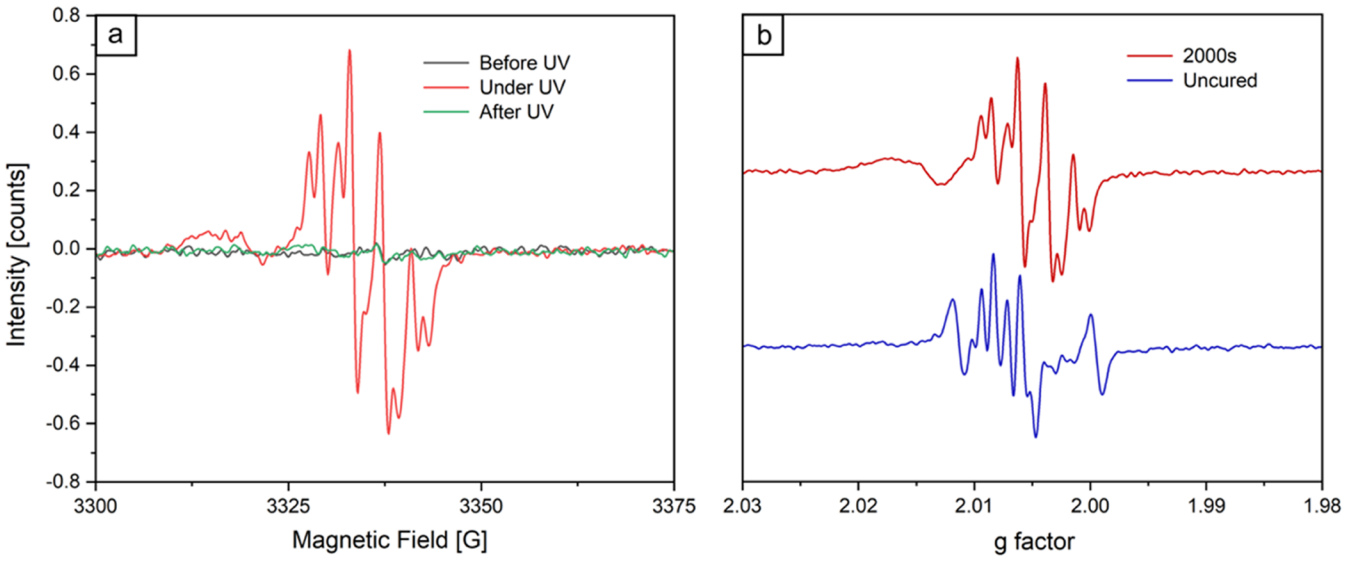

Figure 5. (a) EPR signal of a H-PDMS sample cured for 2000 s. An EPR signal is only detected under UV excitation. (b) Comparison of the EPR signal for an uncured sample and one cured for 2000 s, illustrating that the radicals are likely to be different at different stages in the curing. The UV intensity was 95 mW/cm^2.

demonstrate which chemical bond is primarily responsible for the observed material responses or their different contributions during curing. To clarify the bonding mechanisms in our PhotoCAN elastomers, we used solid-state magic angle spinning NMR analysis of the products to clarify the changes in chemical bonding with increasing UV curing time.

High field measurements were made of the mixture of PDMS molecules, before curing, of the photoinitiator, and of the H-PDMS after different curing times (120, 480, 960, 2000 s). Both ^{1}H and ^{13}C NMR spectra were recorded (Figures 3 and 4). The following results were mainly obtained from ^{13}C NMR: The peaks of the aromatic ring in the photoinitiator (128.56, 130.11, 132.62, and 134.66 ppm) decrease from 480 to 2000 s, and some unidentified products appear in the overcured samples. The C═O peak (203.35 ppm), C−OH peak (76.25 ppm), and $-CH_3$ peak (28.72 ppm) of the photoinitiator gradually decrease and finally almost disappear in the overcured sample, indicating that the photoinitiator is continuously being consumed during the curing process. A small new peak appears at 190 ppm in the overcured sample, which may be aldehyde, a degradation byproduct of the photoinitiator.[18]

The two peaks related to the vinyl group (131.86, 139.45 ppm) only appear in the uncured sample and do not appear in any of the cured samples, indicating that the vinyl in the system is rapidly depleted, consistent with a previous report.[19] The C signals on the side chains of thiol-PDMS (16.85, 27.78, and 28.41 ppm) decrease with curing time and almost disappear in the overcured samples. In contrast, additional peaks at 17.35, 19.34, 23.7, 26.81, and 35.58 ppm appear with curing, and their intensities do not change with UV illumination time. The peak at 35.58 ppm is assigned to C−S−C*−C−C-Si. The peaks related to carbon α to disulfide (C−S−S, 42.35 ppm) and carbon β to disulfide (C*−C−S-S, 23.2 ppm) become more prominent in the sample cured for 960 s and gradually increase over time. Together these observations suggest that the thiol rapidly reacts with vinyl to form a C−S bond, followed by a slower, continuous reaction under UV illumination to form a disulfide bond until finally all thiols are consumed.

With the help of the ^{13}C assignments described above, the peaks of ^{1}H spectra can be addressed with a 2D ^{1}H−^{13}C heteronuclear multiple-quantum correlation (HMQC) experiment, enabling the protons directly attached to carbons to be assigned. The corresponding plots are shown in the Supporting Information, Figures S2 and S3. Using these correlations, we identified the H peak as being adjacent to the sulfur-bearing C in the ^{1}H spectrum in Figure 4.[20] Peak a is associated with the C−S bond, which retains the same intensity after the first UV illumination. Peaks b and c are indicative of the generation of disulfide in the system. Notably, the disulfide bond does not become visible until after curing for 960 s at a flux of 3.5 mW/cm^2.

Summarizing the NMR results, there appear to be two distinct mechanisms involved during UV curing: a relatively fast mechanism and one much slower. The fast reaction is the thiol−ene reaction, in which the vinyl groups are completely consumed within 120 s (at a UV intensity of 3.5 mW/cm^2). The slower reaction is the formation of disulfide bonds. Therefore, in the early stages of the reaction, the active bonding is primarily due to the formation of C−S bonds. Thereafter, the number of C−S bonds remains approximately constant, while the number of disulfide bonds increases continuously.

The rheological data also indicate that the elastomer can be switched by UV throughout the curing process. Correlating the changes observed by NMR and the rheological changes, it can be concluded that in the early stages of the reaction, most of the mechanical response is associated with breaking of the C−S bonds under UV excitation.

3.3. EPR Measurements. The NMR data provide evidence for changes in chemical bonding occurring during curing, but as the measurements were made without simultaneous UV illumination, they provide no information about the reactions occurring during illumination. Such reactions are usually considered to be initiated by free radical reactions, but few papers have shown direct evidence for this. To obtain direct evidence, we conducted in situ EPR tests under UV illumination on samples cured for 120, 480, 960, and 2000 s. Each EPR measurement takes approximately 30 s. As illustrated in Figure 5(a), the EPR results provide direct evidence that the response under UV is driven by a radical-initiated reaction. In the absence of UV, there is no signal from any radicals, but immediately upon UV illumination, there is a clear signal indicative of the presence of radicals. The signal then disappears when the UV is turned off, confirming that the radicals are only generated by the UV exposure and have a short lifetime, less than the 30 s EPR collection time. Interestingly, comparing the EPR signals at different curing times in Figure 5(b), the shape of the radical signal changes between the early and late stages of curing, indicating that the radicals generated during UV illumination change as curing proceeds. Unfortunately, because of the complexity of even this simplest polymer system, it is currently not possible to identify the specific types of radicals formed.

Nevertheless, these findings provide insight into the underlying mechanism of the photoCAN system and suggest that radical

https://doi.org/10.1021/acs.macromol.3c01841
Macromolecules XXXX, XXX, XXX−XXX

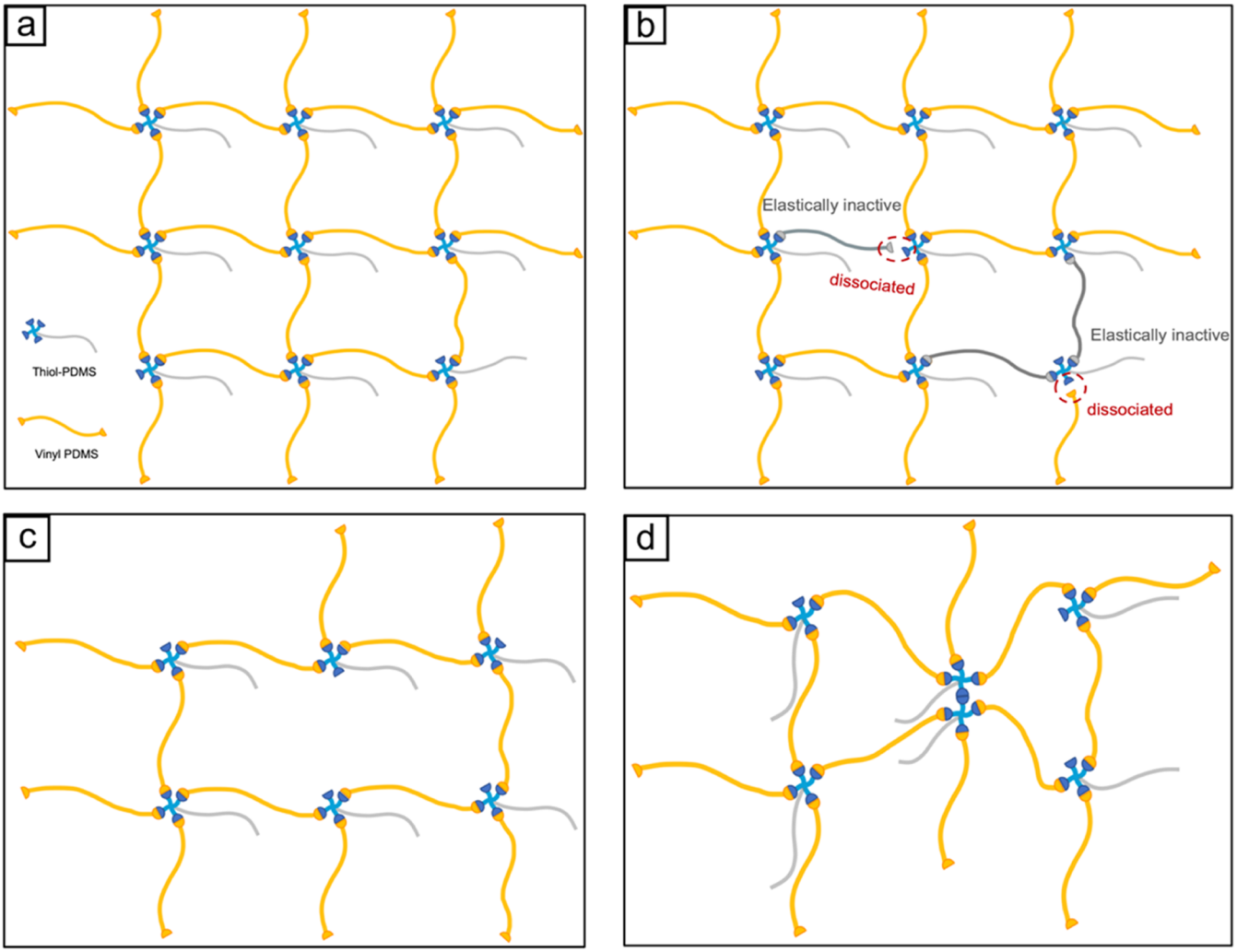

Figure 6. Schematic of the H-PDMS network: (a) without UV illumination, (b) under UV illumination, (c) when only C−S bonds form the network, and (d) the formation of disulfide bonds in the network at later times.

generation and subsequent reaction play a crucial role in the cross-linking of the PDMS network.

4. DISCUSSION

In understanding the molecular reactions involved in covalently adaptive network polymers, it is useful to classify them based on their different responses to external stimuli. The first are associative CANs, in which an intermediate is generated during the reaction of the dynamic bonds. A new chemical bond is formed before the old bond is broken, maintaining the overall integrity of the polymeric network. The second category are dissociative CANs, in which dynamic bonds break under external stimuli and recombine to form new chemical bonds, resulting in a loss of network integrity and decrease in G'. As will be shown by the discussion of the observational data, the PhotoCAN materials can exhibit a combination of both types of network behavior, suggesting that they can be manipulated by the design of appropriate polymer structure.

PhotoCANs exhibit many of the characteristics of dissociative CANs since the rheological data is characterized by dynamic breaking and reforming bonds under UV indicative of the number of chemical bonds and integrity of the network decreasing under stimulation, causing a significant decrease in G'. This behavior is observed by both S-PDMS and H-PDMS elastomers (Figure 1).

Figure 6 is a schematic representation of the H-PDMS network structure consisting of vinyl-terminated PDMS and a PDMS copolymer possessing 4 thiols. The vinyl-terminated PDMS is represented by the telechelic oligomers (shown in yellow). The thiols on the PDMS concentrate at one end of the chain and have an average functionality of 4, so we represent it as a four-arm oligomer with a dangling chain. We distinguish between two types of chain connections: cross-links and junctions. As shown in Figure 6(a), where the functional groups chemically react and integrate into the network is a cross-link. Branch points of multiple functional groups are junctions. Only junctions with a coordination larger than 2 can form network structures. With these definitions, the network strands are the molecular chains between two junctions.

Figure 6(b) is a schematic of the H-PDMS under UV illumination. When exposed to UV, the C−S bonds break, causing a portion of the networked molecular chains to become elastically inactive. This results in an elongation of the network strands, leading to an observed decrease in G'. After the UV is turned off, these functional groups reconnect, and the integrity and connectivity of the network is restored.

https://doi.org/10.1021/acs.macromol.3c01841
Macromolecules XXXX, XXX, XXX−XXX

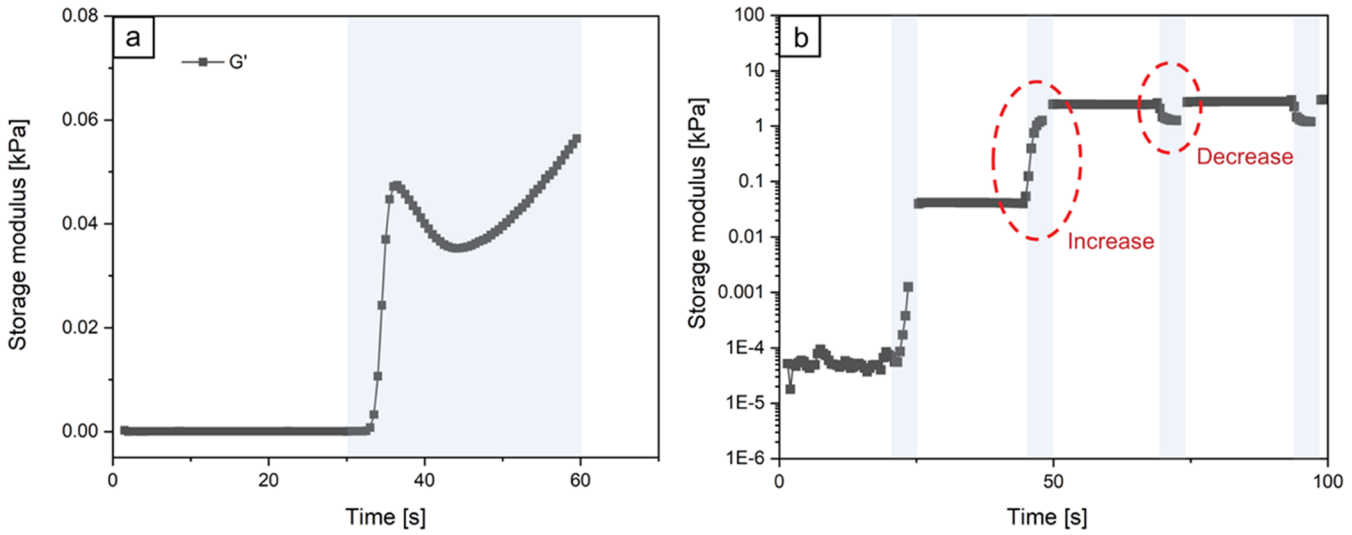

Figure 7. Photoswitching behavior at the earliest stage of the S-PDMS curing for a 30 s UV exposure (a) and for 5 s exposure (b).

Figure 6(c,d) shows schematics of how disulfide bonds affect the network structure. As the curing reaction progresses to the later stages, the thiols slowly react with each other to form disulfide bonds. As shown in Figure 6(d), when two 4-arm oligomers are linked by a disulfide bond, they transform into a junction with a coordination of 6. This results in a shortening of the network strand, causing an increase in G'.

This analysis regarding the network structures is equally applicable to S-PDMS. The network structures of H-PDMS and S-PDMS are very similar; the distinctions between them are the incorporation of SM21 in S-PDMS, which results in longer network strands. Second, the lower concentration of thiols in SMS22 leads to a functionality of 3 in S-PDMS. Consequently, the overall elastic modulus of S-PDMS is lower than that of H-PDMS. Additionally, due to the lower concentration of thiol and vinyl groups in the system, the consumption rate of functional groups in S-PDMS is slower, resulting in an extended lifetime.

However, it is still notable from the data in Figure 1(a,c) that although the G' approaches a maximum value and the switching amplitude decreases with UV, G'' continues to respond. As the maximum value of G' indicates that no further cross-link formation occurs, this behavior suggests that there is a second bonding reaction occurring under UV. This phenomenon has also been found previously in systems without excess thiol[21] when there is no response in G' but only an increase in G'' with UV. This was attributed to a dynamic exchange of disulfide bonds under UV. In our system, we believe that when G' no longer increases, all of the thiols involved in the reaction have formed disulfide bonds or, alternatively, oxidized. After this, some photoinitiator remains so that free radicals generated under UV illumination can drive the dynamic exchange reaction and result in a continued increase in G''. We consider this reaction to be the second type of dynamic chemical bond reaction in the system, a process which we have characterized as an "associative reaction" since it has no influence on G'. The first type of dynamic chemical bond reaction, previously mentioned, is the "dissociative reaction" caused by the cleavage of C−S bonds where these C−S bonds refer to the carbon−sulfur bond in sulfides.

To test this hypothesis, we conducted further experiments by adjusting the ratio of vinyl to thiol in H-PDMS from 1:1 to 1:8. As evident from Figure S4, when the vinyl to thiol ratio was 1:1, no significant decrease in G' under UV was observed. It was only in the case of the thiol excess that G' responded. However, as depicted in Figure S5, the formulation with a 1:1 ratio still exhibits a response in G'' to UV exposure, supporting the proposed hypothesis.

During the earliest stages of curing of S-PDMS, another phenomenon was observed. It is illustrated in Figure 7(a), which is an expansion of the first 60 s of Figure 1(a). With UV on, G' exhibits an almost linear rise, followed by a small peak at 5 s of curing, at which point there is a slight drop, and then continues to rise at a slower rate. To investigate this further, the duration of UV irradiation was shortened to 5 s to let the UV switch fall within the time range of this small peak (Figure 7(b)). Prior to reaching the maximum value of this small peak, each time the UV was switched on, G' would rise. However, after the maximum value, G' would show only a decrease under UV illumination. This small peak was not observed with the H-PDMS, possibly because the reaction in H-PDMS is too fast to be captured. Taken in conjunction with the reaction's dependency on an excess of thiol (Figure S4 and ref 15), the mechanisms of the dissociative reaction can be summarized. At the start of the reaction, the thiols rapidly undergo a thiol−ene reaction with the vinyl groups. The concentration of thiyl radicals is not high at this stage; therefore, there is little contribution from the dynamic cleavage of the C−S bonds. Together, this leads to an almost linear initial increase in G'. Subsequently, since the concentration of thiyl radicals in the system gradually increases and more C−S bonds cleave, the rate of increase in G' decreases and the C−S bonds are in a dynamic equilibrium. In some of the previous reports on the C−S bond contributions to CAN reactions, there was also an excess of thiol,[17] consistent with our surmise. This finding also provides a qualitative explanation for why the free radicals in the early and later stages of the curing process, as observed in the EPR results, are different.

In considering these reactions, the possible reactions with oxygen cannot be ignored, as oxygen is known to affect the curing of PDMS. To investigate possible roles of oxygen, rheological tests of S-PDMS under air and nitrogen environments were performed. The results are shown in Figure 8. Comparing G' in air and under nitrogen, there are three main

https://doi.org/10.1021/acs.macromol.3c01841
Macromolecules XXXX, XXX, XXX−XXX

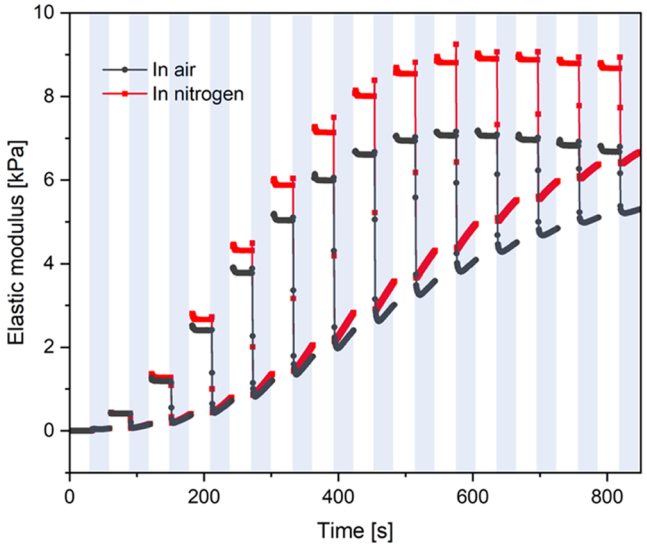

Figure 8. Comparison of G' measurements of S-PDMS performed in air and under nitrogen.

differences. First, the sample cured under oxygen has a lower modulus than that cured in nitrogen, indicating that oxygen inhibits cross-linking presumably through oxygen quenching of radicals and the oxidation of functional groups. Second, the sample cured in air for 800 s exhibits a smaller switching amplitude, which is attributed to more photoinitiator being consumed by oxygen leaving less available for curing. Third, the modulus difference persists until the third cycle of UV radiation, indicating that the reactions involving O_2 have a lower priority than the thiol−ene reaction. In a recent paper,[22] a thiol−ene system with excess thiol has been studied. The result shows that under nitrogen protection, no disulfide bonds are formed within the system. However, when the reaction is conducted under oxygen conditions, disulfide bonds can be detected. From these differences, we conclude that oxygen oxidizes the thiyl radicals, resulting in intermediate products that can no longer undergo chain transfer with the vinyl groups. In essence, this is an oxygen inhibition process.[23] Oxygen also quenches radicals during the polymerization process. Consequently, the cross-link density within the samples exposed to air is lower as indicated by the lower modulus.

Based on our experimental observations, it is possible to form a consistent picture of the chemical bonding changes involved in the UV switching in the photoCAN materials.

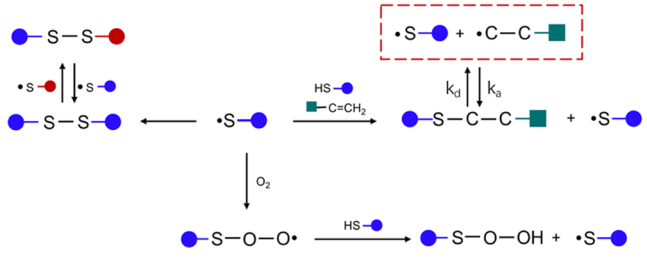

Figure 9. Schematic of the reactions responsible for the UV switching behavior. Under UV, a dissociative reaction takes place between thiyl radicals and thioethers (top right) and an associative reaction occurs between thiyl radicals and disulfides (top left). Competing with them is the irreversible reaction with oxygen.

These are shown in Figure 9. Under UV irradiation, three main reactions occur. The first is the thiol−ene reaction, which proceeds rapidly,[19] quickly forming a cross-link structure. This is consistent with the findings that the vinyl groups were completely consumed in the in situ rheological tests performed under 45 mW/cm^2 UV within 9 s according to NMR data. Additionally, dynamic dissociation occurs when the concentration of thiyl radicals reaches a certain, but not yet determined, value. Therefore, the C−S bond cleavage requires an excess thiyl radical environment in addition to UV or photoinitiator. When the UV illumination is stopped, the dynamic bonds reform, resulting in an accompanying, rapid increase in modulus. The second reaction involves thiyl radicals directly undergoing a termination process to form disulfide bonds. This reaction is slower than the thiol−ene reaction, while the presence of oxygen accelerates it. The third reaction occurs when thiols are oxidized in the presence of oxygen to form peroxyl radicals;[24,25] when excess thiols are present in the system, these peroxyl radicals can be reactivated. The dissociative reaction mentioned earlier involves the C−S bonds, while both the C−S and S−S bonds can take part in the associative reaction.

4.1. Kinetics Model. The response of G' with UV illumination, shown in Figure 1(b,d), can be described in terms of the effective cross-linking density, ν_{eff}, based on the phantom model.[13,26]

$$G' = \left(1 - \frac{2}{f}\right) k_B T \nu_{eff} = \frac{1}{2} k_B T \nu_{eff}$$

where f is the functionality of the junctions, k_B is the Boltzmann constant, and T is the absolute temperature.

For reversible cross-links, when the equilibrium constant of the reaction remains unchanged, ν_{eff} is directly proportional to

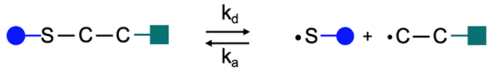

the cross-link density.[27] Therefore, the change in G' caused by turning the UV on and off is directly proportional to the change in the concentration of C−S bonds:

The cleavage of S−C bonds into thiyl- and carbon-centered radicals requires that the concentration of thiyl radicals within the system reaches a certain level to trigger this reaction. Therefore, we hypothesize that the dissociative process is a first-order reaction controlled by the concentration of thiyl radicals. Since the concentration of carbon-centered radicals is always lower than that of thiyl radicals, we postulate that the associative reaction is a first-order reaction controlled by the concentration of carbon-centered radicals. Taken together, we write that

$$\frac{d[C]}{dt} = K_d[S] - K_a[C]$$

where $[C]$ is the concentration of carbon-centered radical, $[S]$ is the concentration of thiyl radical, K_d is the kinetic constant of the dissociative process in the cleavage of C−S bond, and K_a is the kinetic constant of the corresponded associative process.

The concentration of thiyl radicals can be represented by a two-step photoinduced process: the first is the cleavage of the photoinitiator (PI), and the second is the reaction of the initial radicals with thiol to yield high-molecular-weight radicals.

https://doi.org/10.1021/acs.macromol.3c01841
Macromolecules XXXX, XXX, XXX−XXX

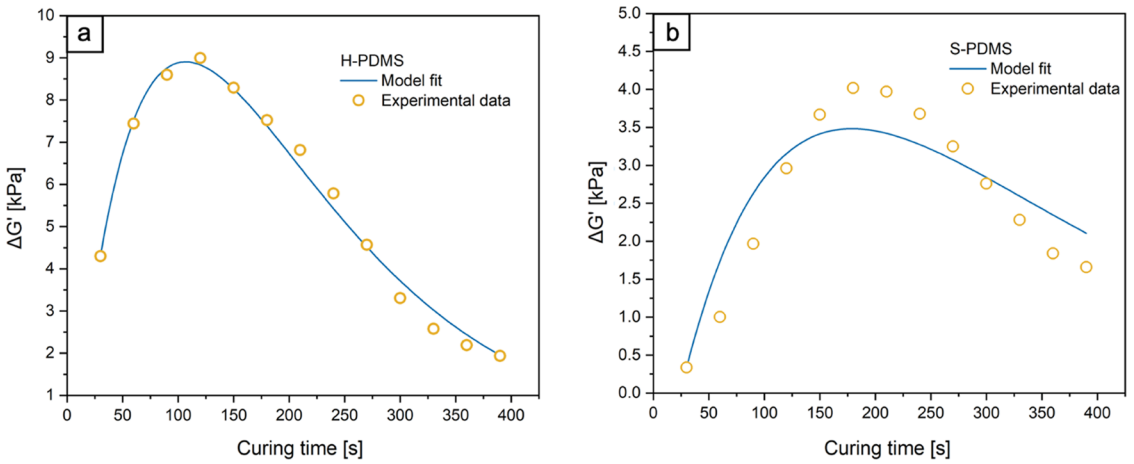

Figure 10. Model fit of $\Delta G'$ for (a) H-PDMS and (b) S-PDMS.

$$\mathrm{PI} \xrightarrow{K_1} 2F^{\bullet}$$

$$F^{\bullet} + \mathrm{RSH} \xrightarrow{K_2} \mathrm{RS}^{\bullet} + F - H$$

In chain initiation reactions, the overall rate of chain initiation can be approximated by the rate of the first step, proportional to the UV intensity, I.[28] Hence,

$$\frac{\mathrm{d}[S]}{\mathrm{d}t} = -2K_1[I]$$

where K_1 is the dissociation constant of the photoinitiator. This leads to a rate equation relating the macroscopic shear modulus and UV-induced chemical reactions

$$\Delta G' = A[C]$$

$$\frac{\mathrm{d}\Delta G'(t)}{\mathrm{d}t} = \frac{K_\mathrm{d}}{A} e^{-2K_1 t} - K_\mathrm{a}\Delta G'(t)$$

Using this model to fit the modulus change, $\Delta G'$, of the H-PDMS, an excellent fit is obtained, Figure 10(a), with the values: $\frac{K_\mathrm{d}}{A} = 266.5$, $K_\mathrm{a} = 0.0101$, and $K_1 = 0.00507$. The model not only fits the mechanical response to UV over the entire curing process, but the rate constant K_1 for the photoinitiator reaction is close to those previously reported.[29]

The fit of the same model to the S-PDMS curing data (Figure 10(b)) is not as good and yields $\frac{K_\mathrm{d}}{A} = 0.0715$, $K_\mathrm{a} = 0.00647$, and $K_1 = 0.00323$. We attribute the poorer fit to a combination of factors associated with the more complex structure of the S-PDMS. The H-PDMS contains only one type of thiol-PDMS, SMS42, which has an f ranging from 3.08 to 6.38 (we adopted an average $f = 4$). The S-PDMS also consists of two different types of thiol-PDMS oligmers. One is SM21, in which both ends of the PDMS chain are thiol-terminated, serving as a chain extender to increase the length of the network strands. The other is SMS22, with f between 1.55 and 3.15. As a functionality of at least 3 is topologically required to form a network, SM21 and a certain amount of SMS22, are incapable of effectively forming a network structure due to the limited number of thiol groups. This complexity is not captured in the model, and correspondingly, the fit to the experimental data is not as good. Nevertheless, the underlying competing rates of the dissociation and association reactions describe the functional form of the G' changes with UV.

5. CONCLUSIONS

The mechanisms responsible for UV-induced photoswitching in photoCAN elastomers have been studied using a combination of MAS solid-state NMR and both in situ EPR and rheological measurements. The rheological and EPR data reveal that the mechanical moduli respond rapidly to UV illumination, a process driven by the formation of free radicals. NMR data demonstrated both C−S and S−S dynamic bonding throughout the curing process, whereas S−S bonds only exist in the later stages. Based on the measurements, we propose that three chemical reactions occur under UV. Among these, the reverse thiol−ene reaction, induced by excess thiol and photoinitiator, results in the abrupt drop of G' under UV illumination. A model, based on the kinetics of the associative and dissociative reactions, successfully relates the change in the modulus produced by UV to the UV curing time.

Our research shows that the thiol−ene reaction has the potential to create both dissociative and associative CANs by controlling the ratio of vinyl and thiol; an excess of thiol is required for a dissociative CAN but not for an associative CAN. To render photoCANs adaptable to a broader range of application scenarios, it is necessary to optimize the photo-CAN to achieve a larger response and exhibit this behavior over a longer time. As the experimental data and analysis presented in this paper indicate, this can be achieved by maintaining the concentration of thiyl radicals within the system. Potential optimization strategies include suppressing the rate of side reactions other than thiol−ene reactions, thereby reducing the consumption rate of thiol. Alternatively, choosing PDMSs with lower content of functional groups decelerates the reaction rate. However, this approach might compromise the mechanical strength of the elastomer. Another possible strategy would be to externally supplement the system with thiol, thus increasing the concentration of thiyl radicals.

■ ASSOCIATED CONTENT

Supporting Information

The Supporting Information is available free of charge at https://pubs.acs.org/doi/10.1021/acs.macromol.3c01841.

Structure of PDMS oligomer (Figure S1); NMR spectra (Figures S2 and S3); and rheological data (Figures S4 and S5) (PDF)

https://doi.org/10.1021/acs.macromol.3c01841
Macromolecules XXXX, XXX, XXX−XXX

AUTHOR INFORMATION

Corresponding Author

David R. Clarke − *School of Engineering and Applied Sciences, Harvard University, Cambridge, Massachusetts 02138, United States;* orcid.org/0000-0002-5902-7369; Email: clarke@seas.harvard.edu

Authors

Miao Huo − *School of Engineering and Applied Sciences, Harvard University, Cambridge, Massachusetts 02138, United States;* orcid.org/0009-0008-7350-4679

Jerry G. Hu − *Materials Research Laboratory, University of California at Santa Barbara, Santa Barbara, California 93106, United States*

Complete contact information is available at: https://pubs.acs.org/10.1021/acs.macromol.3c01841

Notes

The authors declare no competing financial interest.

ACKNOWLEDGMENTS

Dr. M.H. acknowledges a Postdoctoral Fellowship from Shanghai Jiao Tong University for partial support of her studies at Harvard University. This work was supported by the Harvard MRSEC program of the National Science Foundation under award number DMR 20-11754. The authors are grateful to the MRSEC facilities at both Harvard University and UC Santa Barbara (NSF DMR-2308708) for the use of their shared facilities. The authors are also grateful to Dr. Dylan Barber for comments on the manuscript.

REFERENCES

(1) Podgórski, M.; Fairbanks, B. D.; Kirkpatrick, B. E.; McBride, M.; Martinez, A.; Dobson, A.; Bongiardina, N. J.; Bowman, C. N. Toward stimuli-responsive dynamic thermosets through continuous development and improvements in covalent adaptable networks (CANs). *Adv. Mater.* **2020**, *32* (20), No. 1906876, DOI: 10.1002/adma.201906876.

(2) Kloxin, C. J.; Bowman, C. N. Covalent adaptable networks: smart, reconfigurable and responsive network systems. *Chem. Soc. Rev.* **2013**, *42* (17), 7161−7173.

(3) Van Herck, N.; Maes, D.; Unal, K.; Guerre, M.; Winne, J. M.; Du Prez, F. E. Covalent Adaptable Networks with Tunable Exchange Rates Based on Reversible Thiol−yne Cross-Linking. *Angew. Chem., Int. Ed.* **2020**, *59* (9), 3609−3617.

(4) Kloxin, C. J.; Scott, T. F.; Adzima, B. J.; Bowman, C. N. Covalent adaptable networks (CANs): a unique paradigm in cross-linked polymers. *Macromolecules* **2010**, *43* (6), 2643−2653.

(5) Park, H. Y.; Kloxin, C. J.; Scott, T. F.; Bowman, C. N. Covalent adaptable networks as dental restorative resins: stress relaxation by addition−fragmentation chain transfer in allyl sulfide-containing resins. *Dent. Mater.* **2010**, *26* (10), 1010−1016.

(6) Gotor, C.; García, I.; Aroca, Á.; Laureano-Marín, A. M.; Arenas-Alfonseca, L.; Jurado-Flores, A.; Moreno, I.; Romero, L. C. Signaling by hydrogen sulfide and cyanide through post-translational modification. *J. Exp. Bot.* **2019**, *70* (16), 4251−4265.

(7) Orrillo, A. G.; Furlan, R. L. Sulfur in Dynamic Covalent Chemistry. *Angew. Chem., Int. Ed.* **2022**, *61* (26), No. e202201168, DOI: 10.1088/0964-1726/25/8/084017.

(8) Zhang, B.; Digby, Z. A.; Flum, J. A.; Chakma, P.; Saul, J. M.; Sparks, J. L.; Konkolewicz, D. Dynamic Thiol−Michael chemistry for thermoresponsive rehealable and malleable networks. *Macromolecules* **2016**, *49* (18), 6871−6878.

(9) Ishibashi, J. S.; Kalow, J. A. Vitrimeric silicone elastomers enabled by dynamic meldrum's acid-derived cross-links. *ACS Macro Lett.* **2018**, *7* (4), 482−486.

(10) Cheng, K.; Chortos, A.; Lewis, J. A.; Clarke, D. R. Photoswitchable Covalent Adaptive Networks Based on Thiol−Ene Elastomers. *ACS Appl. Mater. Interfaces* **2022**, *14* (3), 4552−4561.

(11) Chiou, B. S.; Schoen, P. E. Effects of crosslinking on thermal and mechanical properties of polyurethanes. *J. Appl. Polym. Sci.* **2002**, *83* (1), 212−223.

(12) Hill, L. W. Calculation of crosslink density in short chain networks. *Prog. Org. Coat.* **1997**, *31* (3), 235−243.

(13) Zhang, V.; Kang, B.; Accardo, J. V.; Kalow, J. A. Structure−Reactivity−Property Relationships in Covalent Adaptable Networks. *J. Am. Chem. Soc.* **2022**, *144* (49), 22358−22377.

(14) White, T. J.; Natarajan, L. V.; Tondiglia, V. P.; Bunning, T. J.; Guymon, C. A. Polymerization kinetics and monomer functionality effects in thiol− ene polymer dispersed liquid crystals. *Macromolecules* **2007**, *40* (4), 1112−1120.

(15) An, S. Y.; Noh, S. M.; Nam, J. H.; Oh, J. K. Dual Sulfide−Disulfide Crosslinked Networks with Rapid and Room Temperature Self-Healability. *Macromol. Rapid Commun.* **2015**, *36* (13), 1255−1260.

(16) Bongiardina, N. J.; Soars, S. M.; Podgorski, M.; Bowman, C. N. Radical-disulfide exchange in thiol−ene−disulfidation polymerizations. *Polym. Chem.* **2022**, *13* (27), 3991−4003.

(17) Cheng, C.; Zhang, X.; Chen, X.; Li, J.; Huang, Q.; Hu, Z.; Tu, Y. Self-healing polymers based on eugenol via combination of thiol-ene and thiol oxidation reactions. *J. Polym. Res.* **2016**, *23*, No. 110, DOI: 10.1007/s10965-016-1001-x.

(18) Molina-Gutiérrez, S.; Dalle Vacche, S.; Vitale, A.; Ladmiral, V.; Caillol, S.; Bongiovanni, R.; Lacroix-Desmazes, P. Photoinduced polymerization of eugenol-derived methacrylates. *Molecules* **2020**, *25* (15), 3444.

(19) Soars, S. M.; Bongiardina, N. J.; Fairbanks, B. D.; Podgórski, M.; Bowman, C. N. Spatial and Temporal Control of Photomediated Disulfide−Ene and Thiol−Ene Chemistries for Two-Stage Polymerizations. *Macromolecules* **2022**, *55* (5), 1811−1821.

(20) van den Berg, O.; Nguyen, L.-T. T.; Teixeira, R. F.; Goethals, F.; Ozdilek, C.; Berghmans, S.; Du Prez, F. E. Low modulus dry silicone-gel materials by photoinduced thiol−ene chemistry. *Macromolecules* **2014**, *47* (4), 1292−1300.

(21) Yang, H.; Chen, X.; Sun, B.; Tang, J.; Vlassak, J. J. Fracture tolerance induced by dynamic bonds in hydrogels. *J. Mech. Phys. Solids* **2022**, *169*, No. 105083.

(22) Liu, X.; Bai, R.; Guo, Z.; Che, Y.; Guo, C.; Xing, H. Photogeneration of thiyl radicals using metal-halide perovskite for highly efficient synthesis of thioethers. *Appl. Organomet. Chem.* **2022**, *36* (2), No. e6492, DOI: 10.1002/aoc.6492.

(23) Krutkramelis, K.; Xia, B.; Oakey, J. Monodisperse polyethylene glycol diacrylate hydrogel microsphere formation by oxygen-controlled photopolymerization in a microfluidic device. *Lab Chip* **2016**, *16* (8), 1457−1465.

(24) Hawkins, C. L.; Davies, M. J. Generation and propagation of radical reactions on proteins. *Biochim. Biophys. Acta, Bioenerg.* **2001**, *1504* (2−3), 196−219.

(25) Hoyle, C. E.; Lowe, A. B.; Bowman, C. N. Thiol-click chemistry: a multifaceted toolbox for small molecule and polymer synthesis. *Chem. Soc. Rev.* **2010**, *39* (4), 1355−1387.

(26) Cramer, N. B.; Bowman, C. N. Kinetics of thiol−ene and thiol−acrylate photopolymerizations with real-time fourier transform infrared. *J. Polym. Sci., Part A: Polym. Chem.* **2001**, *39* (19), 3311−3319.

(27) Parada, G. A.; Zhao, X. Ideal reversible polymer networks. *Soft Matter* **2018**, *14* (25), 5186−5196.

(28) Moad, G.; Solomon, D. H. *The Chemistry of Radical Polymerization*; Elsevier, 2006.

(29) Dickey, M. D.; Willson, C. G. Kinetic parameters for step and flash imprint lithography photopolymerization. *AIChE J.* **2006**, *52* (2), 777−784.